Journal of Rehabilitation in Civil Engineering 8-4 (2020) 173-196

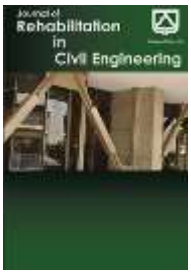

journal homepage: http://civiljournal.semnan.ac.ir/

Investigating the Effect of Pseudo-Static Components on Bridge Structures under Multiple Support Excitations Using Conditional Simulated Records

A. Hosseinnezhad [1] and A. Gholizad [2*]

1. Ph.D. Student, Department of Civil Engineering, University of Mohaghegh Ardabili, Ardabil, Iran.
2. Professor, Department of Civil Engineering, University of Mohaghegh Ardabili, Ardabil, Iran.

Corresponding author: *gholizad@uma.ac.ir*

ARTICLE INFO

Article history:
Received: 12 April 2020
Accepted: 29 July 2020

Keywords:
Long-span bridges,
SVGM,
Pseudo-static response,
SSI.

ABSTRACT

Long-span bridges, as vital structures, play an important role in economic development. Previous studies revealed that the seismic responses of such structures, under non-uniform excitations, are different from the same result due to uniform excitations. Furthermore, the results of several earthquake-damaged bridges showed that their seismic behavior was different from that predicted under uniform excitation and, in some cases; the responses were more than predicted results. Therefore, the damaged bridges under non-uniform excitations were re-analyzed and the obtained results were in good agreement with the recorded outcomes. Considering current bridge designing codes it is clear that almost all of them ignored it and just the Euro Code 2008 prepared some recommendations. It is found that the main reason for the differences in results from the uniform and non-uniform excitations is the spatial variation of earthquake ground motions. Based on the papers three phenomena were introduced for spatial variability of ground motion: the wave-passage, the incoherence, and also the site-response effects. The responses of structures under non-uniform excitations obtained from the superposition of dynamic and pseudo-static components. This paper investigated the seismic behavior of a long-span structure under non-uniform movements to evaluate the most undesirable conditions. So, different soils and load combinations considered and soil-structure effects included. The effect of wave-passage, incoherence, and site-response on the structure was measured and the results were compared with the uniform excitation. The results indicate that the variation in soil condition significantly affects the seismic responses under non-uniform excitations. Also, it is found that the results from uniform excitations with considering soil-structure interactions are remarkably increased. Moreover, the outcomes of analysis under-considered load cases and soil conditions showed that ignoring the spatially varying ground motions may lead to a non-conservative design.

DOI: 10.22075/JRCE.2020.20195.1401

1. Introduction

Earthquake ground movements changes in time and space. One of the usual methods of seismic analyzing structures is to consider time variations and ignore spatial variations. Therefore, the seismic analysis of structures is mainly based on the assumption that the structure vibrates in phase at all supports with constant amplitude everywhere. However, in practice for long-span structures such as bridges, this assumption is inaccurate because the structure experiences different movements at each support during an earthquake [1]. The spatial variation of ground motion (SVGM) is commonly divided into three components: (i) a wave passage effect, (ii) geometric incoherence of the input motions, and (iii) local site conditions. The first component is due to the differences between travel speeds of seismic waves. The second one rises from reflection and refraction of seismic waves when traveling through the ground, the frequency content of the wave changes between support points. And the third one is related to the changes in the local site conditions. As regards, long-span structures such as bridges have multiple supports and different soil conditions cause a different response to the structure. Based on the results observed from asynchronous motion during earthquakes, the spatial variation of ground motions is a complex interaction of all three components, so for analytical simplicity, researchers have divided the phenomenon into these three sources [2]. Several previous studies have shown that the effect of SVGM on the structures cannot be neglected and in some cases was too devastating [3]. To simulate the SVGMs the assumption of stationarity is necessary and the simulation is conducted by a coherency function that models the variation of the ground with a predefined theoretical target power spectral density function (PSDF). To provide temporal non-stationarity, the results are then corrected in time. However, this technique does not consider the spectral non-stationarity of the ground motion. This method is known as unconditioned simulation technique. One of the methods for simulating the seismic ground motion for a given coherency function is the probabilistic conditioning to a real record at a specific site, and this method is called conditional simulation [4-5-6]. To maintain non-stationary properties, the record is split into specific time intervals. However, for an ensemble array generated by conditional simulation, the ensemble variance increases with increasing distance from the simulation point. To resolve the recent problem, the power spectral density (PSD) of the simulated record conditioned to the PSD of the target record in time intervals that predefined [7]. Since 1960s, several researchers have studied the effect of SVGM on the structures by considering the only wave passage effect, that is considering the ground motions travel with a constant velocity on the ground surface without any change in their form [1]. This means that SVGM makes the seismic wave with a time lag to reach far away supports. During the 1970s and 1980s, a dense network of seismography arrays was created, aiming at a precise study of the SVGM and its effect on the responses of various structural systems. After that, the effect of coherency loss and local site effect has been considered in SVGM modeling. Since 1980, the topic of non-uniform excitations has engaged many researchers and valuable papers have been published. Some researchers investigated new formulation for SVGM and also the effect of spatially varying ground motions on

long-span structures [9-10]. Recently, Apaydin et al. (2016) studied the structural behavior of the Fatih Sultan Mehmet suspension bridge under multi-support earthquake excitations [11]. SVGM was simulated in triple direction for each support of the bridge using a modified stochastic finite-fault technique. In a study by Adanur et al. (2016), Bosphorus suspension bridge studied for the spatial variability effects of ground motions using the response spectrum and a random vibration-based spectral analysis method [12]. Based on the results, it was concluded that the multiple support seismic responses depend on the intensity and frequency contents of power spectral density functions for each random vibration analysis. Falamarz-Sheikhabadi and Zerva (2016, 2017, and 2018) have studied the importance of the SVGM effect and presented new formulation methods [13-14]. Sextos and Papadopoulos (2018) investigated the effect of asynchronous ground motions on the transverse response of base-isolated bridges [15]. They used the un-conditional method to generate correlated time series based on the EC8 spectrum. Various loading scenarios defined and the generated time series imposed on the bridge. The results show that the seismic response of the structure increases by considering SVGMs. Zhong et al. (2018) studied the non-linear behavior of a cable-stayed bridge under spatially varying earthquake ground motions [16]. They used the conditional method to generate correlated ground motions and presented seismic hazard maps to evaluate the effect of spatially varying ground motions parameters. Zhao et al. (2018) compared the seismic response of the bridges with precast segmental and traditional monolithic columns under spatially varying earthquake excitations [17]. The results reveal that when abutments are not considered, the spatially varying ground excitation can dramatically change the relative pounding compared with uniform seismic loading. When abutments are considered in the numerical model, the influence of spatial variations on the bridge-pounding responses becomes less significant. Bas et al. (2018) surveyed the non-linear behavior of the Bosphorus Bridge under multiple support excitations [18]. They used simulated ground motions based on the local site PSDF. The results indicate that the bridge response increased under non-uniform excitations. Jeon et al. (2018) studied the non-linear behavior of retrofitted columns of a reinforced concrete bridge under non-uniform excitations [19]. They concluded that considering spatially varying ground motions increase the probability of failure in some cases. Yurdakul and Ates (2018) investigated the isolated and non-isolated bridge under non-uniform excitations [20]. The wave passage, incoherency, and local site effects considered. The outcomes showed that the SVGMs affect the responses of the structures. Tonyali et al. (2019) studied the seismic behavior of the Quincy Bay suspension bridge under spatially varying ground motions [21]. The results revealed that the seismic wave velocity and soil condition change the responses and in some cases increase them. Shirvand and Parvanehro (2019) investigated the response of a cable-stayed bridge under uniform and non-uniform seismic excitations [22]. They implemented the unconditional method to generate correlated ground motions and modeled the structure using SAP2000. The results concentrated on the Girder moments, Cable forces, and the response of Pylons that show different outcomes for uniform and non-uniform excitation scenarios. Payganeh and Mortezaei (2020) studied the effect of

earthquake rotational components and soil-structure interactions on the seismic behavior of reinforced concrete structures. The results showed that the rotational components effects are considerable [23]. Also, many papers published that focused on the effect of SVGMs on the seismic behavior of the structures, but few papers indicate that which of the SVGMs components is more important compared to others. In the present study, the customary simulation methods introduced by Konakli and Der Kiureghian (2012) were explained and a Matlab code was developed to simulate the correlated arrays [24]. To explore the effect of SVGM on the structures, a prototype CALTRANS bridge was selected, and the finite element model generated by OpenSEES. The simulated arrays imposed on the bridge supports and the results of uniform and multiple support excitations were compared.

2. Spatially Variations in Ground Motion

Considering SVGM studies, three mechanisms cause the spatial variation of ground motion [3]: The difference in arrival times of the seismic waves at different locations, commonly known as the wave passage effect; the change in the shape of the propagating waveform due to multiple scatterings of the seismic waves in the highly inhomogeneous soil medium, referred to as the incoherence effect; and the change in amplitude and frequency content of ground motion at different locations on the ground surface due to different local soil conditions known as the local site effect.

2.1. Presentations of Spatially Variation in Ground Motions

Here, we assume an array of jointly stationary Gaussian acceleration processes that defined at n locations by cross power spectral densities, $G_{kl}(\omega)$, k, l=1, 2,…, n, k $\neq$ l, and auto power spectral densities, $G_{kk}(\omega)$, k=1, 2,…, n. n is the number of separate measurements observed at the same periods Δt. Also, we mentioned that $t_i = i\Delta t$, i= 0… n−1. Problem simplification, it is assumed that n is even, but it is easy to generalize the problem when N is odd [25] (Anderson, 1971). Normally the arrays expressed in terms of the Fourier series [26].

$$a_k(t_i) = A_{0k} + \sum_{p=1}^{\frac{N}{2}-1}\left[A_{pk} * cos(\omega_p t_i) + B_{pk} * sin(\omega_p t_i)\right] + (-1)^i * A_{(\frac{N}{2})k} \quad k = 1,2,\dots,n \qquad (1)$$

In which N is the number of discrete events given at equal time intervals Δt, $\omega_p = \frac{2\pi p}{N\Delta t}$, and $\{A_{pk}\ B_{pk}\}$ are the Fourier coefficients. The Fourier coefficients are jointly Gaussian random variables with zero-mean and uncorrelated for different frequencies, that is, $E\left[A_{pk}\,A_{qk}\right] = E\left[B_{pk}\,B_{qk}\right] = E\left[A_{pk}\,B_{qk}\right] =$ 0 for p $\neq$ q. At frequency ω_p, we have [26]:

$$E[A_{pk}A_{pl}] = E[B_{pk}B_{pl}] = \begin{cases} G_{kk}(\omega_p)\Delta\omega, & if\ k = l \\ Re[G_{kl}(\omega_p)]\Delta\omega, & if\ k \neq l \end{cases} \qquad (2)$$

$$E[A_{pk}B_{pl}] = -E[B_{pk}A_{pl}] = \begin{cases} 0 & if\ k = l \\ -Im[G_{kl}(\omega_p)]\Delta\omega, & if\ k \neq l \end{cases}$$

Therefore, with defined auto-PSDs and cross-PSDs, it can be determined the variances and covariance of all Fourier coefficients. The relation between the cross-PSDs and auto-PSDs of generated arrays at sites k and l is represented as [26]:

$$G_{kl}(\omega) = \gamma_{kl}(\omega) * |G_{kk}G_{ll}(\omega)|^{0.5} \qquad (3)$$

In which the spatial variation of the ground motion in the frequency domain is presented by the coherency function which defined as $\gamma_{kl}(\omega)$.

2.2. Approximation of Statistical Properties of Specified Realizations

Consider, $a_k(t_i), i = 1, \dots, N$ represents a record at location *k*. The following equation is an approximation of the auto power spectral density of the record at the location [27]:

$$I_{kk}(\omega_p) = \frac{N\Delta t}{4\pi}\left(A_{pk}^2 + B_{pk}^2\right) = \frac{\Delta t}{\pi N}\left|\sum_{i=1}^{N} a_k(t_i) exp(i\, t_i\, \omega_p)\right|^2 \quad (4)$$

Where the Fourier coefficients are given by $A_{pk} = 2\sum_{i=1}^{N}\frac{a_k(t_i)\cos((\omega_p t_i)}{N}$ and $B_{pk} = 2\sum_{i=1}^{N}\frac{a_k(t_i)\sin((\omega_p t_i)}{N}$ for $p=1,\dots,\frac{N}{2}$. Also, $A_{0k} = \sum_{i=1}^{N}\frac{a_k(t_i)}{N} = \overline{a_k}$ *and* $A_{(N/2)k} = \sum_{i=1}^{N}\frac{(-1)^i a_k(t_i)}{N}$.

Also, for each pair of acceleration time histories, $a_l(t_i)$ and $a_k(t_i)$, the smoothed cross periodogram is a steady approximation of the cross power spectral density of the related processes. The following equations represent the real and imaginary sections of the cross periodogram, I_{kl} [27]:

$$Re\left[I_{kl}(\omega_p)\right] = \frac{N\Delta t}{4\pi}\left(A_{pk}A_{pl} + B_{pk}B_{pl}\right) \quad and \quad Im\left[I_{kl}(\omega_p)\right] = \frac{N\Delta t}{4\pi}\left(A_{pk}B_{pl} - A_{pl}B_{pk}\right) \quad (5)$$

2.3. Coherency

Consider, $a_k(t_i), i = 1, \dots, N$ represents a record at location *k*. The following equation is an approximation of the auto power spectral density of the record at the location [27]:

From the smoothed cross-spectrum of the motions between the two stations *j* and *k* the coherency of the seismic ground motions are obtained and normalized regarding the related power spectra as [28-29]:

$$\gamma_{jk}(\omega) = \frac{S_{jk}(\omega)}{\sqrt{S_{jj}(\omega) * S_{kk}(\omega)}} \quad (6)$$

$\gamma_{jk}(\omega)$, is a complex number; the square of the absolute value of the coherency and the subscript *n* in the frequency has been omitted for convenience. So, the coherence is written as [30]:

$$\left|\gamma_{jk}(\omega)\right|^2 = \frac{\left|S_{jk}(\omega)\right|^2}{S_{jj}(\omega)S_{kk}(\omega)} \quad (7)$$

is a real number and gives values $0 \leq \left|\gamma_{jk}(\omega)\right|^2 \leq 1$. It is customary to write coherency as [30]:

$$\gamma_{jk}(\omega) = \left|\gamma_{jk}(\omega)\right| exp\left[i\theta_{jk}(\omega)\right] \quad (8)$$

with

$$\theta_{jk}(\omega) = tan^{-1}\left(\frac{I[S_{jk}(\omega)]}{R[S_{jk}(\omega)]}\right) \quad (9)$$

Which named as phase spectrum; the real and imaginary part for Equation (7) is defined as R and I, respectively.

2.4. Spatial Variability Models

The mathematical definition for the coherency is called coherency model. Two types of coherency models have been presented by numerous researchers: empirical and semi-empirical. The first equation about coherency in the field of earthquake engineering was introduced by [31]. The expression was:

$$|\gamma(\varepsilon, \omega)| = \exp\left[-k\left(\frac{\omega * \varepsilon}{V_s}\right)\right]^v \quad (10)$$

where k and v are constant and V_s, is an appropriate shear wave velocity. Der Kiureghian and Neuenhofer (1992), present a model for the expression of the coherency function in which all the parameters that

influence the SVGM are considered [32]. This model represented below:

$$\gamma_{kl}(\omega) = |\gamma_{kl}(\omega)| * exp\{i * [\theta_{kl}^{wp}(\omega) + \theta_{kl}^{sr}(\omega)]\} \quad (11)$$

In which $|\gamma_{kl}(\omega)|$ defines the incoherence effects, $\theta_{kl}^{wp}(\omega)$ describes wave-passage effects, and the local site effects characterized by $\theta_{kl}^{sr}(\omega)$.

One of the most famous equations extensively used by researchers is introduced by Luco-Wang (1986):

$$|\gamma(\varepsilon, \omega)| = exp\left[-\left(\frac{\alpha d_{kl}\omega}{v_s}\right)^2\right] \quad (12)$$

Where the distance between point's k and l is titled d_{kl}, the average shear wave velocity is v_s, and α is incoherence parameter that can be estimated from data gathered in [26, 32]. The phase angle caused by wave-passage effect is defined as [40]:

$$\theta_{kl}^{wp}(\omega) = -\frac{\omega d_{kl}^{L}}{v_{app}} \quad (13)$$

In which v_{app} and d_{kl}^{L}, are the surface apparent wave velocity and horizontal distance in the longitudinal direction of propagation of waves respectively. The phase angle caused by the site-response effect is introduced as [33]:

$$\theta_{kl}^{sr} = tan^{-1}\frac{Im|H_k(\omega)H_l(-\omega)|}{Re|H_k(\omega)H_l(-\omega)|} \quad (14)$$

where $H_k(\omega)$, is the frequency response function (FRF).

2.5. Conditional and Unconditional Simulation of Ground Motions

Seismic accelerograms have non-stationary specifications in the time and frequency domains. To simulate the seismic motion, it is necessary to assume those that are stationary. Therefore, the seismic ground motion is studied in small intervals and it can be claimed that they are almost stationary. Since the seismic ground motion is the result of the superposition of random waves arriving from intermittent ruptures, according to the central limit theory, the record can be assumed to be Gaussian. There are two methods for generating stationary Gaussian arrays. Vanmarcke and Fenton (1991) titled the methods as "unconditional" and "conditional" simulation techniques. For unconditioned method, simulated records are generated from a specific (Power Spectral Density) PSD, whereas for conditioned simulation technique simulated records are conditioned to a real record which observed at a site [4].

2.6. Unconditional Simulation

Here, the problem is simulating arrays of zero-mean stationary Gaussian acceleration time series at locations with known site conditions and for a predefined spatial variability model, while a random conception of the array at one site is given. The site characteristics are defined by the FRFs (Fourier's Response Functions) of the related soil-columns and the spatial variability of the ground motion is represented by a coherence function. Now to solve the problem we need to simulate Fourier coefficients at discrete frequencies and separate locations. For any location, to get a similar acceleration time-history, the simulated Fourier coefficients are replaced in Equation (1). Then for a given auto-power spectral density, the site FRFs and the coherency function, the sets of Fourier coefficients at each frequency are accomplished by sampling from a joint Gaussian distribution. To clarify the procedure, consider we are going to simulate a set of zero-mean acceleration time series at stations $k = 1,2,\dots,n$ with defined site

FRFs, $h_k(\omega)$ and based on a coherence function, and an observed record at a site sampled at N points. Assume $X_p = [A_{p1}\, B_{p1} \dots A_{pn}\, B_{pn}]$ represents the set of Fourier coefficients at frequency ω_p for the n locations and considers $\sum pp$ represents the $2n*2n$ covariance matrix of the mentioned coefficients. Consider that the joint distribution of the zero-mean Gaussian vector X_p is completely defined by the covariance matrix. The elements $\sum_{pp,ij}$ of this matrix are determined using Equation (2). The latter equations $G_{kk}(\omega_p), k = 1,2, \dots, n$ involve the auto-PSDs, and the $G_{kl}(\omega_p), k, l = 1,2, \dots, n\ k \neq l$ cross-PSDs. Let assume the similar spectral density introduced for the ground motion at all sites; the auto-power spectral density for a pair of locations is defined by:

$$G_{ll}(\omega) = G_{kk}(\omega)\frac{|h_l(\omega)|^2}{|h_k(\omega)|^2} \quad (15)$$

The complete set of auto-PSDs is obtained based on the estimated auto-PSD of the known realization and the site FRFs by using the Equation (15). Then by using Equation (3) a complete set of cross power spectral densities based on the auto power spectral densities and the coherence function. Given the matrix of covariance, the sample vectors are generated as $x_p = L_p^T z_p$ where L_p is an upper triangular matrix as $L_p^T L_P = \sum pp$ and z_p is a vector of $2n$ uncorrelated standard normal variables. Cholesky decomposition method is applied to get, L_p. To generate the time histories for all locations Equation (1) is used after sampling at all frequencies, $\omega_p = \frac{2\pi p}{N\Delta t}, p = 1,2, \dots, \frac{N}{2}$.

2.7. Conditional Simulation

Assume the situation in which several records are known at some stations and the other records for other stations need to be generated based on the known records and a predefined coherence function. As with the unconditional simulation method, it is assumed that all the properties of the site locations are expressed in terms of its FRF. Hereon, the Fourier coefficients of the records at the target stations have been taken from a joint Gaussian distribution obtained by stochastic conditioning. Based on the symbolization method of the former section, we assume a zero mean set of Fourier coefficients $X_p = [A_{p1}\, B_{p1} \dots A_{pn}\, B_{pn}]$ at frequency ω_p for all n sites and the $2n$ x $2n$ covariance matrix $\sum pp$ of these coefficients. We divide X_p into two partitions, $X_{p1} = [A_{p1}\, B_{p1} \dots A_{pm}\, B_{pm}]$, $m < n$ and , $X_{p2} = [A_{pm+1}\, B_{pm+1} \dots A_{pn}\, B_{pn}]$ where $k = 1,2, \dots, n$ are the locations with known records. Introduced as conditional distribution of X_{p2} given $X_{p1} = x_{p1}$ is jointly normal with mean:

$$M_{(p,2|1)} = \sum pp, 21\,(\sum pp, 11)^{-1} x_{p1} \quad (16)$$

and covariance matrix

$$\sum(p, 22|11) = \sum pp, 22 - \sum pp, 21\,(\sum pp, 11)^{-1} \sum pp, 12 \quad (17)$$

where $\sum pp, ij$ explains the sub-matrix of $\sum pp$ defining the covariance of vectors X_{pi} and, X_{pj}.

Assume that at location k=1, the record is given in time domain and the conditioned records at locations k=2,…,n is supposed to be simulated. The 2(n − 1)-D joint Gaussian distribution of the Fourier coefficients for the target n – 1 locations is defined by the conditional mean vector and covariance matrix in Equations (16) and (17), respectively. In which, $x_{p1} = [A_{p1}\ B_{p1}]$ is the Fourier coefficients of the known records. For each frequency, $\omega_p = \frac{2\pi p}{N\Delta t}, p = 1, \dots, \frac{N}{2}$, a

specimen set of Fourier coefficients for target points is taken as follows $x_{p2} = M_{(p,2|1)} + L^T_{(p,2|1)} z_p$, where $L^T_{(p,2|1)}$ is an upper triangular matrix, $L^T_{(p,2|1)}$ $L_{(p,2|1)}$ $=\sum(p, 22|11)$, and $z_p$is a 2 $(n-1)$ vector of uncorrelated standard normal variables. It is worth noting that sampling is not necessary for p = 0, since for $\omega_p = 0$ all records are completely related, and the Fourier coefficients at all locations are like each other. Given the vectors x_{p2} at all frequencies, acceleration time histories at the target locations are obtained by using Equation (1).

3. Numerical study

In this section, to explore the effect of SVGM, a reinforced concrete bridge with a box-girder deck and single-column bent are selected. The properties of the deck and the columns are taken from a PEER Center prototype bridge portfolio that includes several types of common decks and column bent solutions designed for California seismic exposure [34]. Figure 1 shows the plan, piers view, and sections of the bridge respectively. The bridge has a curved plan shape with a radius equal to 304.8 m. The elastic properties of the deck are shown in Table 1. The specifications of the concrete and steel materials that assumed for the bridge are shown in Table 2. The characteristics of the columns and abatements are presented in Tables 3 and 4 respectively. The bridges are modeled by the OpenSEES platform. Figure 2, illustrates a schematic view of the FE models [35]. The elastic-beam-column elements used to make the deck and assumed it remains un-cracked. The properties of the deck gathered in Table 1.

Table 1. The deck specifications.

Area	A	5.72 m^2
Compressive Strength	$f^{/}_{c.dec}$	34.47 MPa
Elasticity Modulus	E	27,596 MPa
Shear Modulus	G	11,498 MPa
Moment of Inertia About y-Axis	I_z	2.81 m^4
Moment of Inertia About z-Axis	I_y	53.87 m^4
Torsional Moment of Inertia	J_t	6.03 m^4
Prestressing Force	F_P	31,136 kN

Table 2. Material properties.

confined concrete		
Compressive strength	$f^{/}_{cc}$	46.63 MPa
Strain at $f^{/}_{cc}$	ε_{cc}	0.0089
Crushing strength	f_{cu}	38.72 MPa
Crushing strain	ε_{cu}	0.0365
Elasticity modulus	E_c	24,692 MPa
Tensile strength	f_t	2.76 MPa
unconfined concrete		
Compressive strength	$f^{/}_{co}$	27.6 MPa
Strain at $f^{/}_{co}$	ε_{psco}	0.002
Crushing strength	f_{pcu}	0.0 MPa
Sapling strain	ε_{sp}	0.005
steel		
Yield strength	f_{ye}	470 MPa
Elasticity modulus	E_s	200,000 MPa

In order to make a better estimation, the deck divided into 50 segments. The forced-based fiber-section beam-column element used to model the bridge columns [36]. The connection between the columns and the deck are modeled by rigid links. Recently Tondini and Stojadinovic (2012) studied the

non-linear behavior of the bridge under uniform excitation, but did not consider the SVGM effects [37]. Furthermore, to achieve more accurate results in the present study, the finite element model is developed. Amjadian and Agrawal (2017) studied the dynamic characteristics of the bridge [38]. They assumed the deck remained rigid and used a 2D model of the bridge. To ensure the accuracy of the finite element model, the dynamic characteristics of the bridges compared with the results of the mentioned papers.

To model the abutments, non-linear zero Lenght elements are used and the required specifications are listed in Table 4 [39-40]. The mentioned elements assigned to the FE model in all three directions. Finally, the columns at the ground level fixed. Based on section 3, a Matlab code is developed and correlated arrays are generated.

Table 3. Moment and shear capacity of columns.

Yield curvature φ_y $(\frac{rad}{m})$	0.003976
Yield moment M_y (kNm)	6,650
Plastic moment M_p (kNm)	8,985
Nominal shear strength V_n (kN)	6,278
$M_p/V_n\, d$	1.17
Shear span to depth ratio longitudinal $H_{col}/2d$	2.75

Table 4. Properties of the abutments.

Back wall with	8.23 m
Wing wall with	3.96 m
$K_{abt}\ long$	101,811 kN/m
$P_{bw}\ long$	3,860 kN
$K_{abt}\ trans$	243,753 kN/m
$P_{bw}\ trans$	1,656 kN
ρ	1,760 kg/m^3
v_s	150 m/s
E_{soil}	110,972 MPa

The averages shear wave velocity obtained from PEER report number, 2012/08, and shown in Table 5 [41]. Also, the apparent wave velocity calculated by the formula introduced by Toki and Yanabu [42]. In this study assumed that the epicenter is far away from the bridge that means, $V_s = V_{app}$. To explore the effect of SVGM on the dynamic response of the bridge, five excitations scenarios are considered (Table 6). Case 1 means a uniform excitation; Cases 2 and 3 contain two SVGM components, the wave-passage, and incoherency. The difference between cases 2 and 3 is the rate of incoherency. In case 2 a weak incoherency and in case 3 a strong incoherency considered to separate the effect of wave-passage and incoherency on the seismic response of the bridge under non-uniform excitations. Cases 4 and 5 include site-response effects with weak and strong incoherency rates. So, it is possible to investigate the effect of all SVGM components on the bridge. To simulate the arrays, the Northridge record is used and the conditional simulation method was implemented to generate the correlated ground motions. Based on the bridge plan, there are five simulation points with distances, 36.6, 82.3, 128, 173.7, and 210.3 meters from the known point of the simulation. To consider the local site effects, it is assumed that the abatements are situated on the hard soil (Site Class, A, and B, Table 5), Two columns at coordinates 36.6 and 173.7 m are located on the medium soil (Site Class, C, and D, Table 5) and columns with coordinates 82.3 and 128 m are situated on the soft soil condition (Site Class, E, Table 5). The incoherence parameter varies from 0.0 to 1.0, which has been introduced by numerous researchers [30].

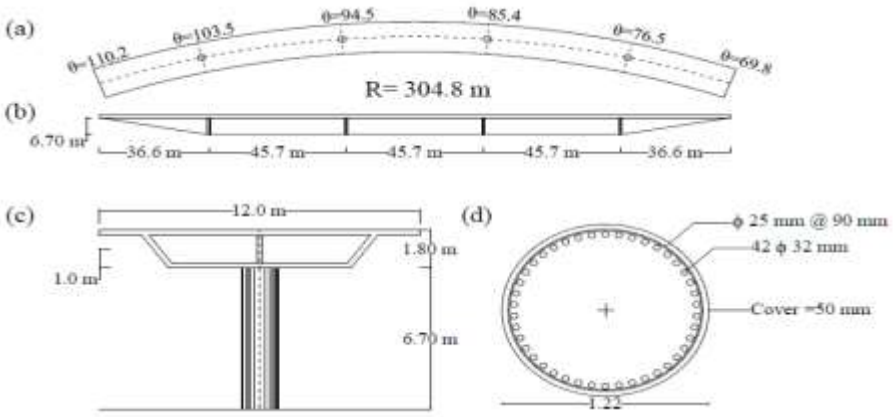

Fig. 1. (a) Plan, (b) View and (c) Section of the deck and columns.

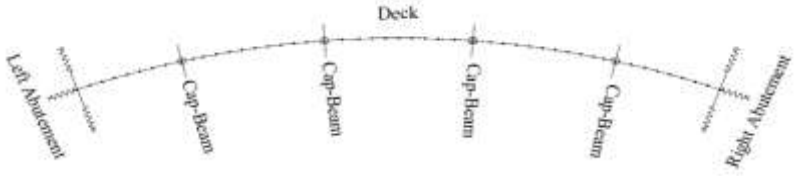

Fig. 2. Schematic representation of the bridge.

Figures 3 and 4 illustrate the simulated acceleration time series for cases 2 and 3 respectively. The corresponding acceleration response spectrums depict in Figures 5 and 6. From the acceleration response spectrums, it is clear that increasing the incoherence parameter caused a little change in the simulated time series. Moreover, the mean spectrum intensity reduced for load case 3. It is logical because with increasing the incoherency, the seismic wave scattered and the corresponding seismic energy reduced.

Table 5. Average Shear and Apparent wave velocity.

Site Class	Soil Profile Name	$V_{s30} = V_{app}$
A	Hard Rock	>1500 m/s
B	Rock	760 to 1500 m/s
C	Very Dense Soil and Soft Rock	360 to 760 m/s
D	Stiff Soil	180 to 360 m/s
E	Soft Soil	<180 m/s

Table 6. Considered scenarios of ground motions spatial variability.

Different load cases and soil conditions	
case 1	uniform motions
case 2	non-uniform excitations considering incoherence ($\alpha = 0.2$) and wave passage effects
case 3	non-uniform excitations considering incoherence ($\alpha = 0.4$) and wave passage effects
case 4	non-uniform excitations considering incoherence ($\alpha = 0.2$), wave passage and local site effect
case 5	non-uniform excitations considering incoherence ($\alpha = 0.4$), wave passage and local site effect

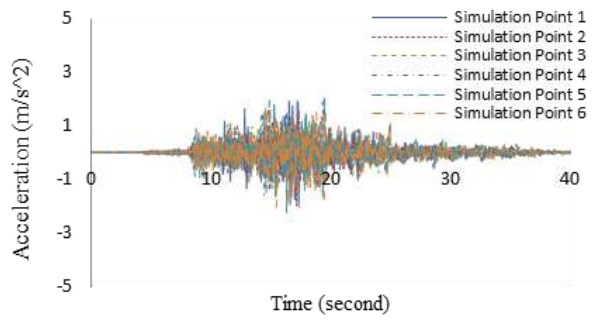

Fig. 3. Simulated Records for Case 2.

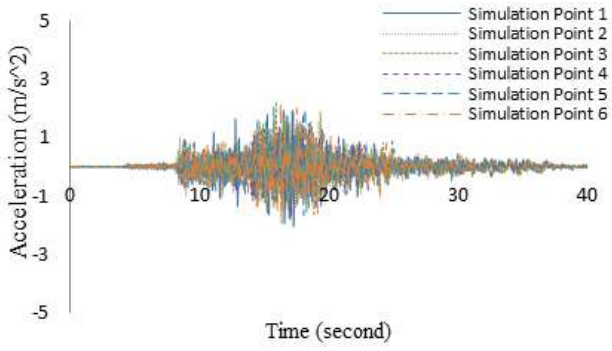

Fig. 4. Simulated Records for Case 3.

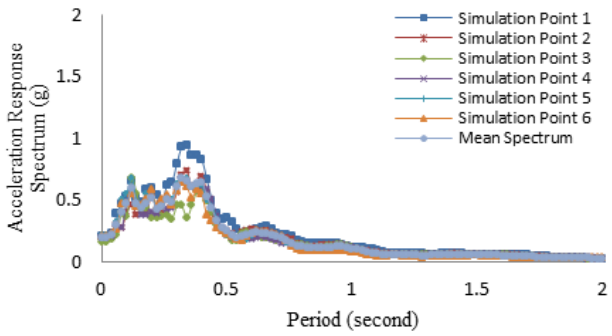

Fig. 5. Acceleration Response Spectrum (Case 2).

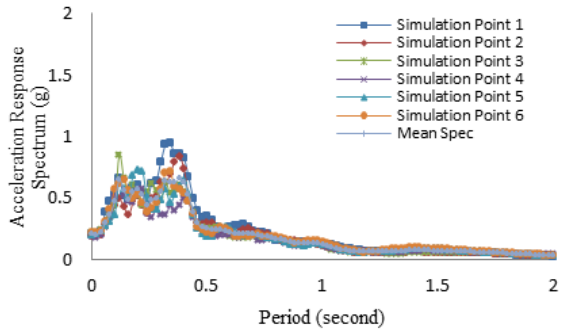

Fig. 6. Acceleration Response Spectrum (Case 3).

Figures 7 and 8 illustrate the simulated acceleration time series for cases 4 and 5 respectively. The corresponding acceleration response spectrums depict in Figures 9 and 10. For load cases 4 and 5 the local site effects added to the simulation process. From the simulated time series, it is obvious that the local site effects significantly increased the maximum acceleration responses. In all cases, the first simulation point is the known record. Considering the response spectrums, it is clear that simulated records are reasonably consistent with the known (original) record. Based on Figures 7 and 8 it seems that increasing the incoherency caused the maximum acceleration to be reduced. Regarding simulated records, it can be seen that the local site effects, significantly increased the peak ground acceleration at simulation points, 3 and 4 that assumed to be located on the soft deposits. The maximum accelerations of simulated records based on cases 4 and 5 (Figures 7 and 8) are almost 0.5g and 0.4g respectively while for the cases 2 and 3 (Figure 3 & 4) are about 0.3g. The same results obtained from acceleration response spectrums (Figures 5, 6, 9 & 10) that confirmed the accuracy of the simulated records. Also, from the outcomes of record simulation, it is found that the local site condition (soft deposits) significantly increased the maximum acceleration, and increasing the incoherency lead to decreasing in seismic energy. The first four mode shapes and corresponding periods and frequencies illustrated in Figure 11.

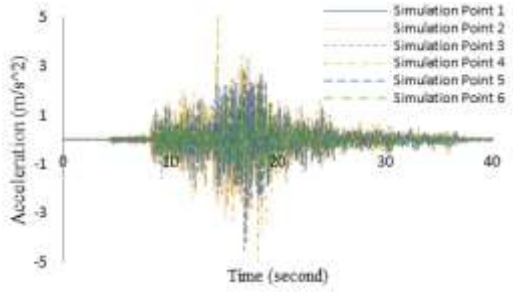

Fig. 7. Simulated Records for Case 4.

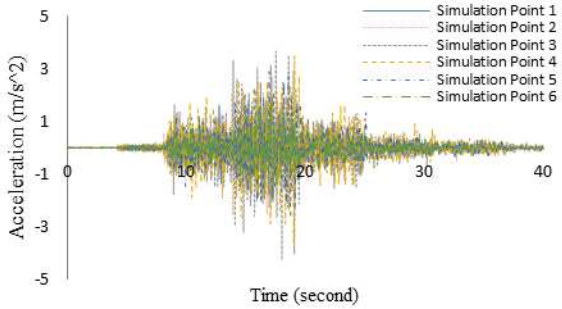

Fig. 8. Simulated Records for Case 5.

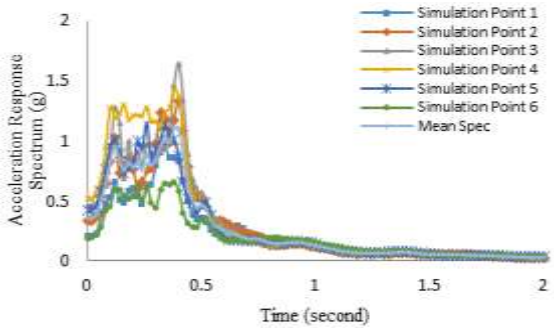

Fig. 9. Acceleration Response Spectrum (Case 4).

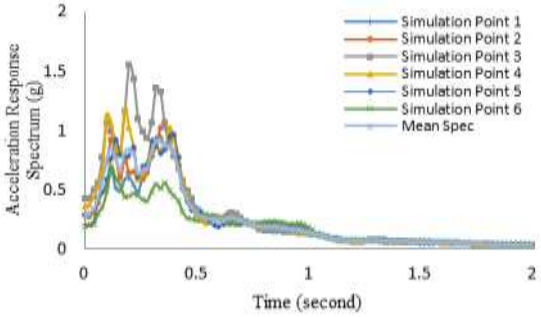

Fig. 10. Acceleration Response Spectrum (Case 5)

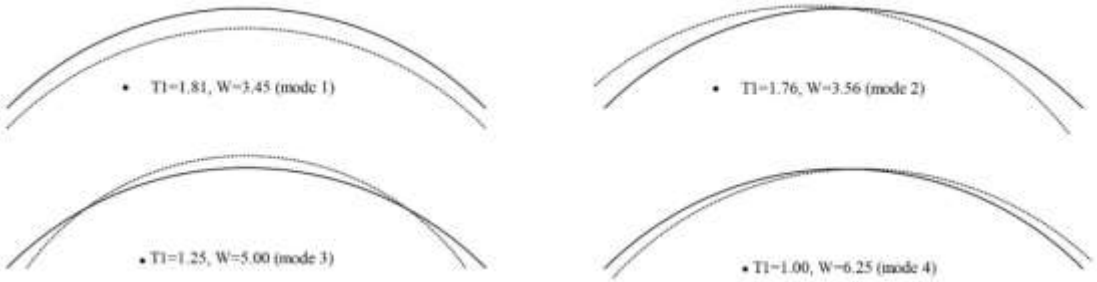

Fig. 11: The first four mode shapes.

4. Results and Discussions

To describe the behavior of the bridge under non-uniform excitations some important responses selected and discussed. So, the base shear at columns support, the axial force of columns, drift ratio at the top of the columns, and the deck displacement were chosen and monitored under uniform and non-uniform excitations.

4.1. Base Shear

Figures 12 from (a) to (p), illustrate the corresponding base shear under different load and soil scenarios. For load cases 2, 3, and 5 the outcomes are lower than the results obtained under load case 1. Interestingly, the soft soil deposits increased the base shears under load case 4, as the values obtained are greater than those of uniform excitation.

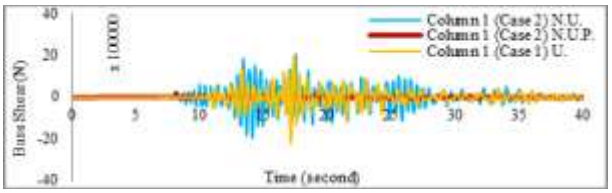

(a)

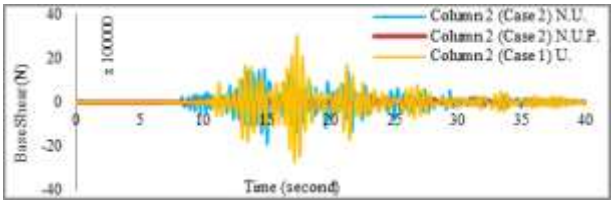

(b)

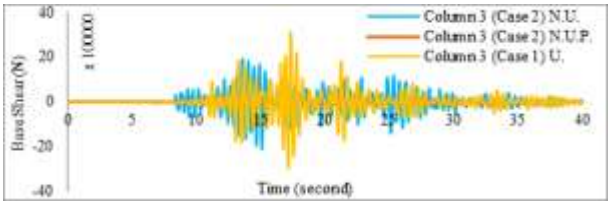

(c)

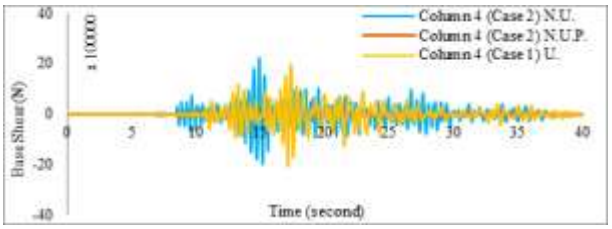

(d)

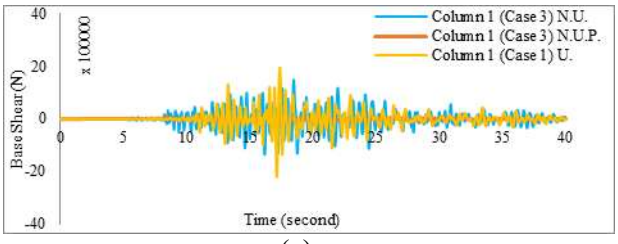

(e)

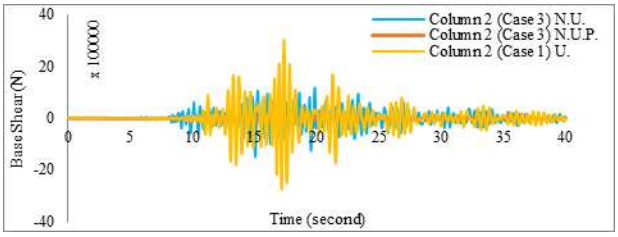

(f)

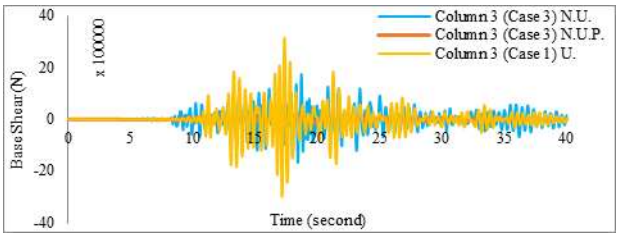

(g)

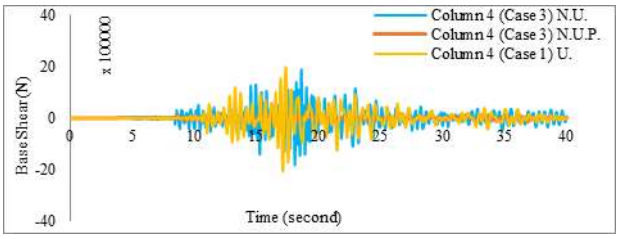

(h)

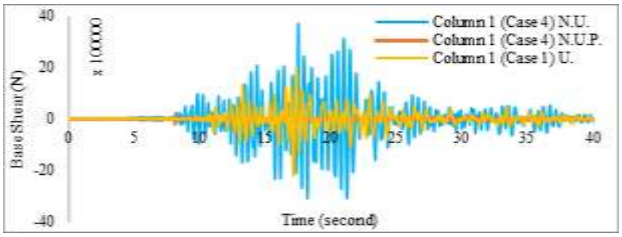

(i)

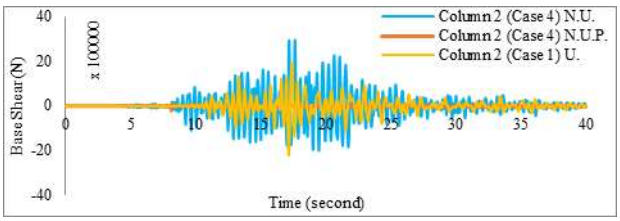

(j)

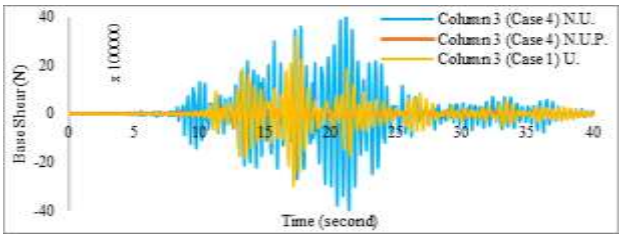

(k)

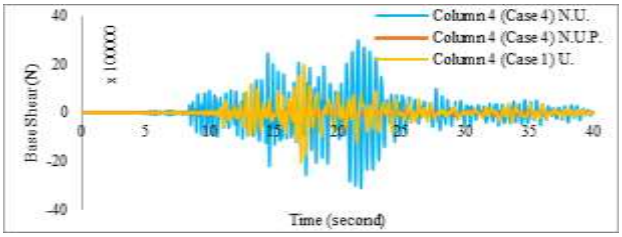

(l)

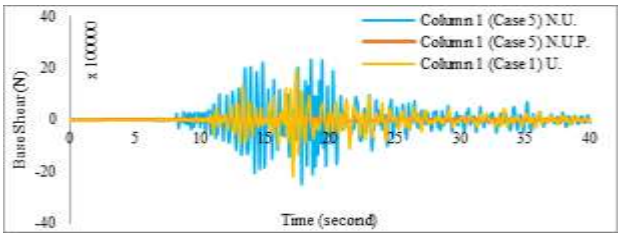

(m)

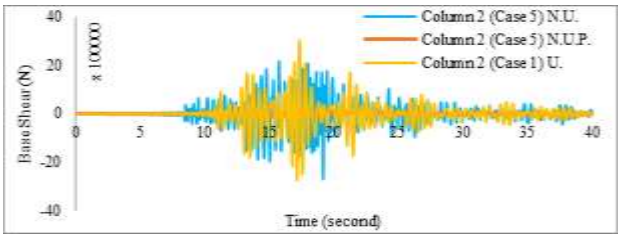

(n)

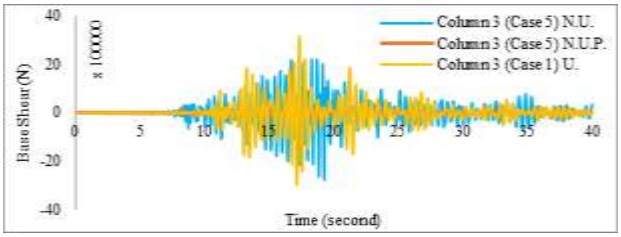

(o)

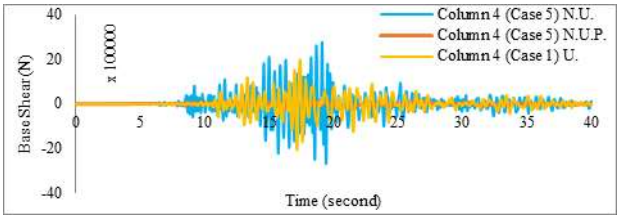

(p)

Fig. 12. Variation of base shear for the Columns, N: non-uniform, P: pseudo-static, U: uniform responses.

In another word, for uniform soil conditions, the base shear result from uniform excitations is always more than the same results obtained from non-uniform excitations. Considering the results from cases 2 and 3, and also cases 4 and 5 it can be seen that by increasing the incoherency the responses from non-uniform excitations reduced. It means that for a strong incoherency condition the traveling wave scattered and the exciting energy reduced. To better understand the SVGMs effects, it customary to decompose the pseudo-static components from the total response. To do it, the mass of the deck and the damping ratio were considered to be zero. Consequently, from results, it is clear that the pseudo-static components play no important role in the base shear responses. So, it can be concluded that the base shear is not sensitive to non-uniform excitations in uniform soil conditions. Regarding the Figures, it is clear that the responses obtained from pseudo-static components are very little and can be neglected.

4.2. Axial Force

The results revealed that the axial force response is sensitive to spatially varying ground motions. The total trend of the results shows that soft soil conditions decrease the response of the pseudo-static components. Considering Figures 13 (i and k) and (j and l), it is obvious that the axial forces caused by pseudo-static components for columns situated on the soft soil condition are fewer than the same results on stiff soil. Comparing the results obtained from cases 4 and 5 indicate that the axial force response increases by increasing the incoherency. Furthermore, the responses due to uniform excitations are very close to non-uniform results under cases 4 and 5 while for cases 2 and 3 the responses obtained from uniform excitations are more than the results from non-uniform excitations. However, the maximum response due to non-uniform excitations occurred under case 4 that is in full agreement with the results of base shear response. Also, total non-uniform responses under case 5 reduced while the contribution of the pseudo-static components increased. This means that despite decreasing excitation wave energy and total response under non-uniform excitation, the rate of response due to pseudo-static components is increased and its effect on axial force is visible.

Table 8. The Response ratios of axial force for different load cases.

	Column 1		Column 2		Column 3		Column 4	
	$\frac{P.}{N.}$	$\frac{N.}{U.}$	$\frac{P.}{N.}$	$\frac{N.}{U.}$	$\frac{P.}{N.}$	$\frac{N.}{U.}$	$\frac{P.}{N.}$	$\frac{N.}{U.}$
Case 2	0.25	0.86	0.08	0.83	0.27	0.64	0.44	0.89
Case 3	0.24	0.99	0.11	0.88	0.22	0.77	0.38	0.87
Case 4	0.44	0.85	0.41	0.90	0.47	0.79	0.55	0.80
Case 5	0.45	0.82	0.34	0.97	0.33	0.85	0.73	0.68

U, uniform – N, non-uniform – P, pseudo-static

Therefore, it can be concluded that the axial force is highly sensitive to changes in the coherency. This issue is very important for cable-stayed structures.

The maximum response ratios of axial force under different load cases for all columns are presented in Table 8. It is obvious that the maximum responses caused by load case 4 in which the wave-passage and local site effects with weak incoherency considered. Also, considering wave-passage, local site effects, and strong incoherency remarkably increased the response ratio of the pseudo-static component to total responses under non-uniform excitations.

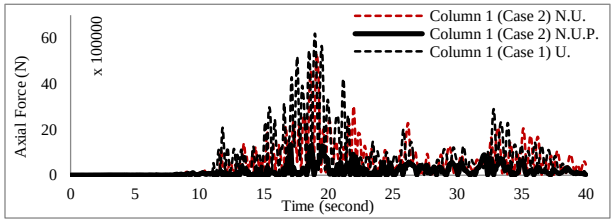

(a)

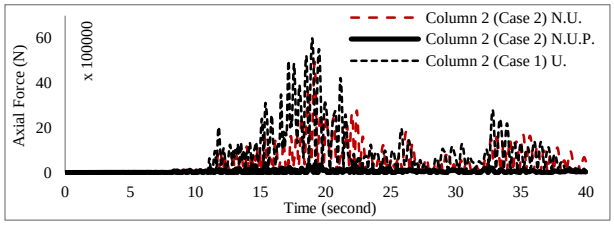

(b)

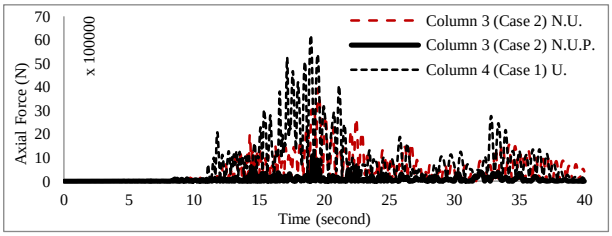

(c)

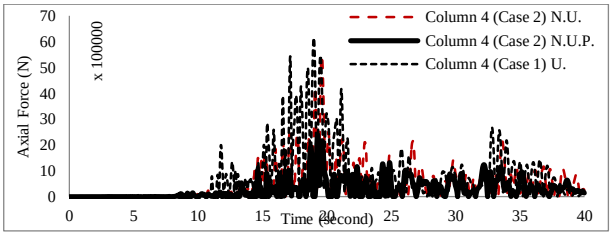

(d)

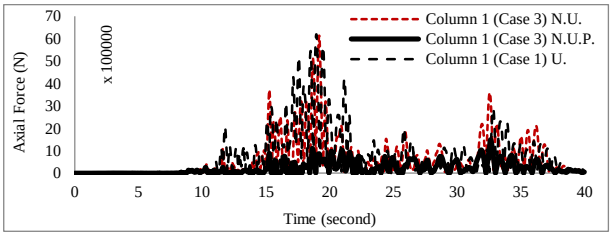

(e)

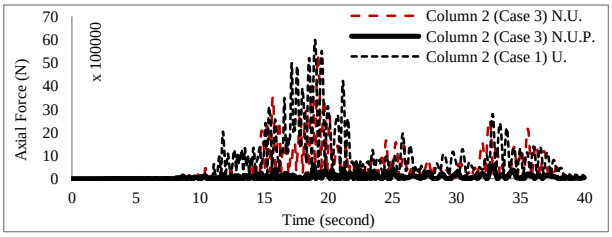

(f)

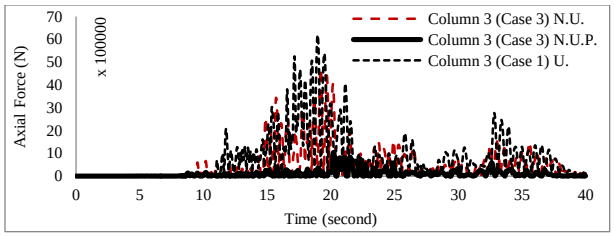

(g)

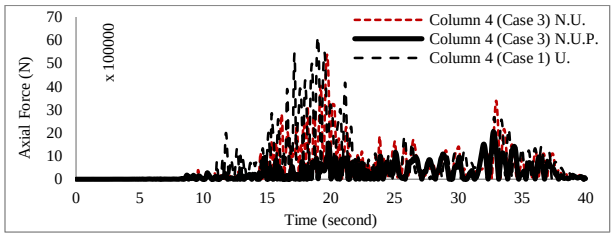

(h)

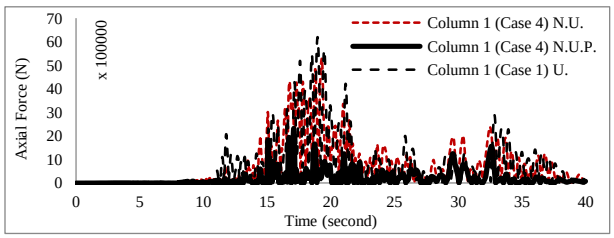

(i)

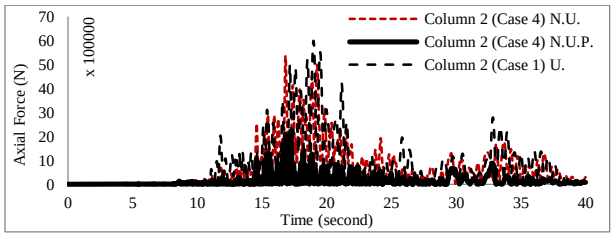

(j)

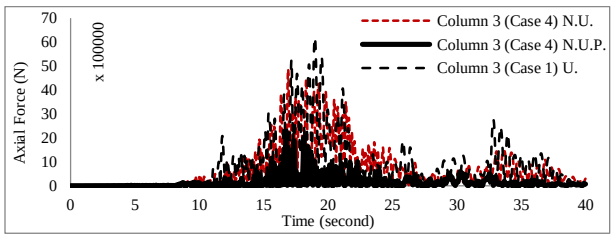

(k)

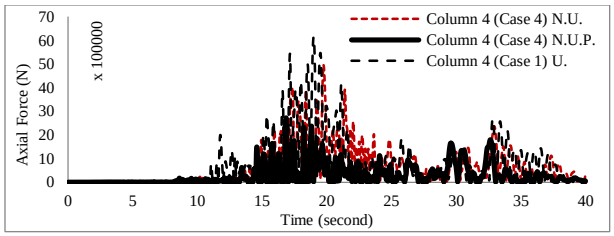

(l)

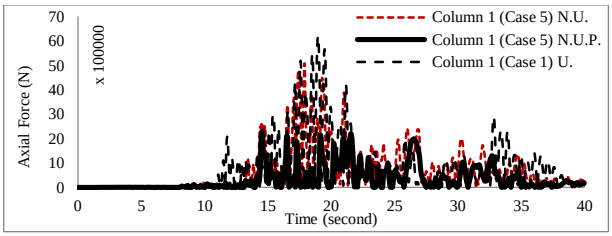

(m)

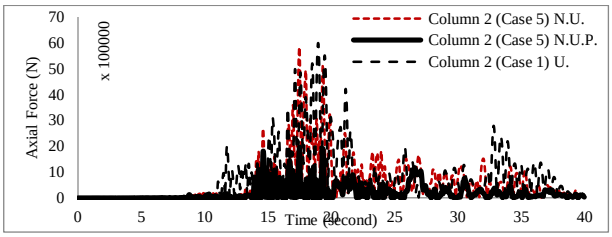

(n)

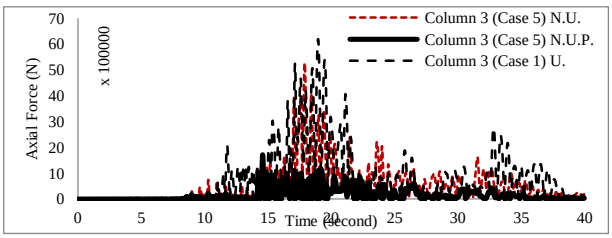

(o)

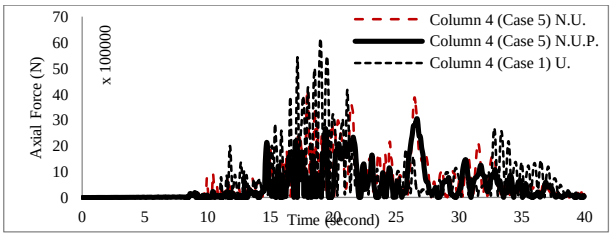

(p)

Fig. 13. Variation of axial force for the Columns, N: non-uniform, P: pseudo-static, U: uniform responses

4.3. Drift Ratio

In this section, the drift ratio of the columns under non-uniform and uniform excitations examined and illustrated in Figures 14. Also, the ratios of responses represented in Table 9. The results show that the responses are sensitive to the pseudo-static components as the highest response rate occurred under load cases 4 and 5. By comparing the results of load cases 2 and 3 with the load cases 4 and 5, it is clear that soil conditions have an

important role in enhancing the responses. Besides, the results show that in some cases the responses under non-uniform excitations are very close to those under uniform excitation. Considering Table 9, the maximum response ratios occurred under load case 5.

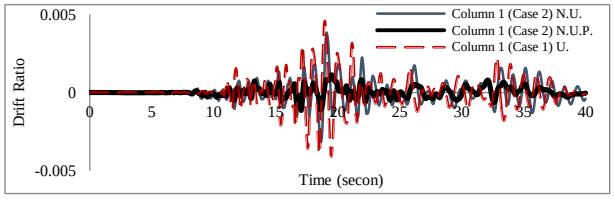

(a)

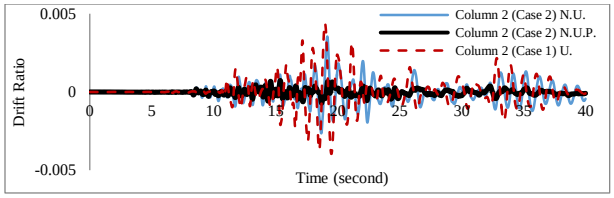

(b)

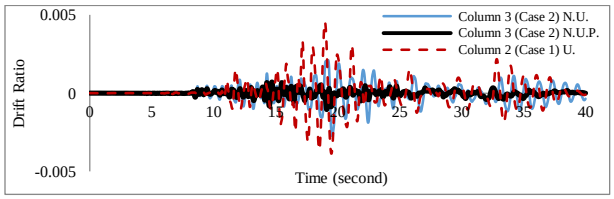

(c)

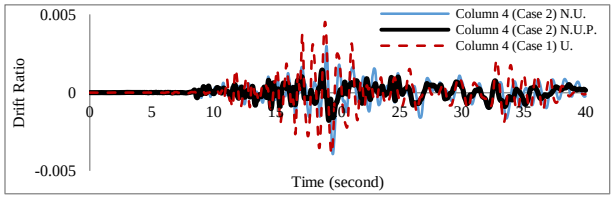

(d)

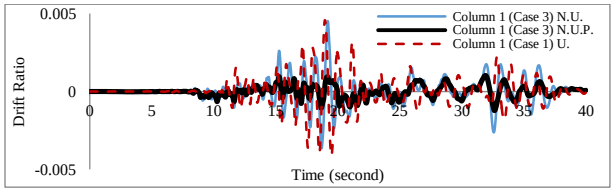

(e)

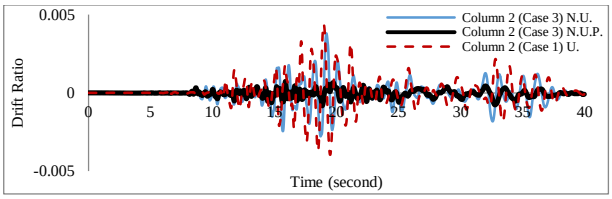

(f)

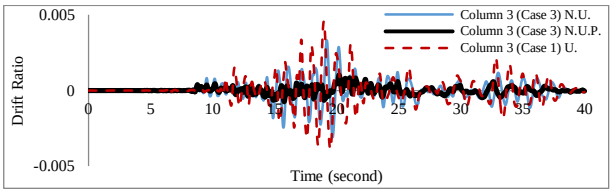

(g)

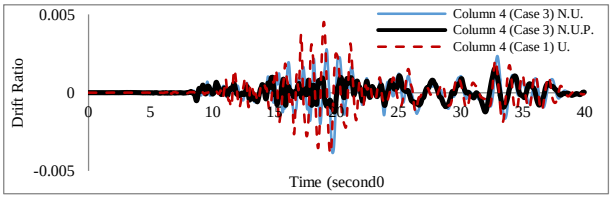

(h)

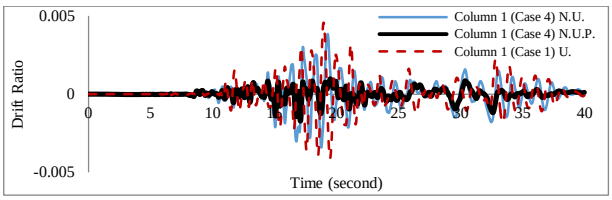

(i)

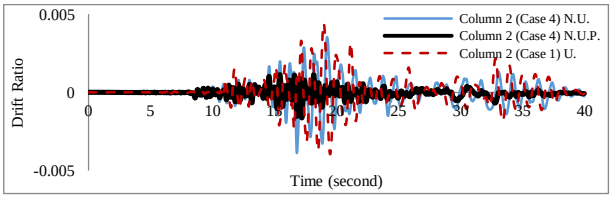

(j)

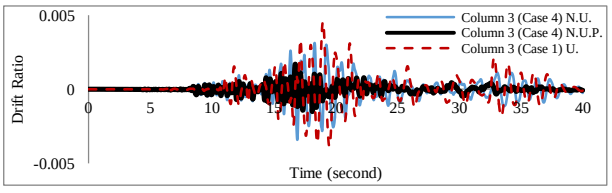

(k)

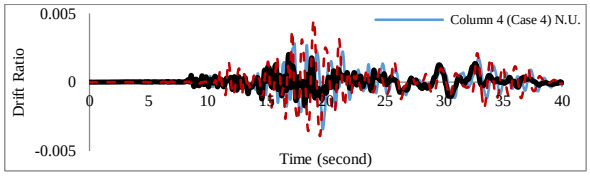

(l)

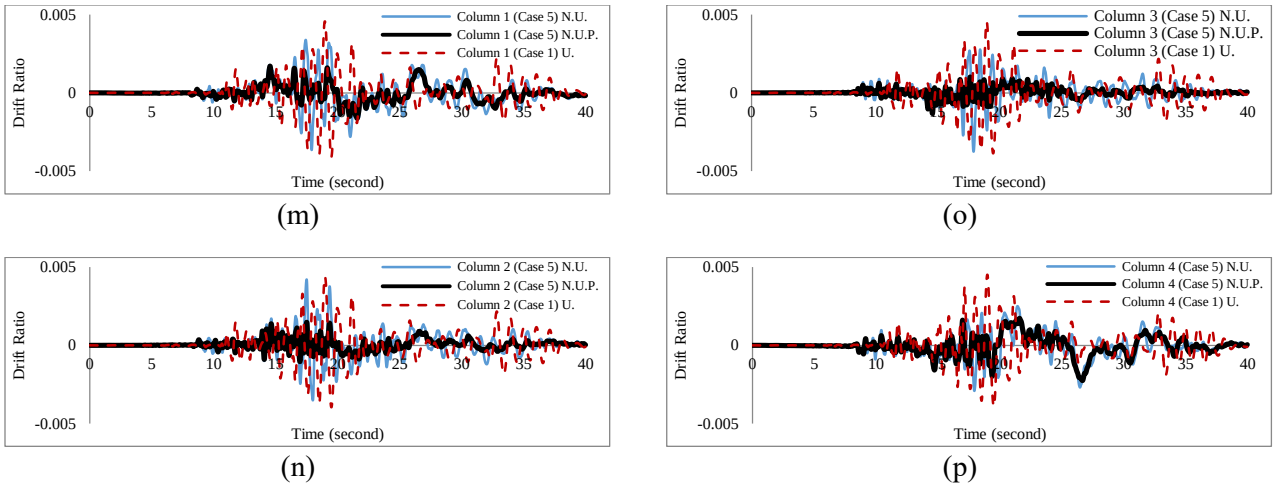

Fig. 14. Variation of drift ratio for the Columns, N: non-uniform, P: pseudo-static, U: uniform responses

Table 9. The Response ratios of drifts for different load cases.

	Column 1		Column 2		Column 3		Column 4	
	$\frac{P.}{N.}$	$\frac{N.}{U.}$	$\frac{P.}{N.}$	$\frac{N.}{U.}$	$\frac{P.}{N.}$	$\frac{N.}{U.}$	$\frac{P.}{N.}$	$\frac{N.}{U.}$
Case 2	0.29	0.84	0.21	0.81	0.34	0.46	0.49	0.66
Case 3	0.23	0.99	0.19	0.87	0.31	0.73	0.55	0.61
Case 4	0.25	0.84	0.32	0.80	0.54	0.69	0.71	0.62
Case 5	0.50	0.74	0.35	0.96	0.37	0.61	0.69	0.55

U, uniform – N, non-uniform – P, pseudo-static

According to the results, the soft soil conditions increase the total dynamic response while reducing the effects of the pseudo-static components. Comparing Figures 14 (m) and (o) with Figures 14 (n) and (p) show that the drift response is sensitive to incoherency and wave-passage. In general, it can be seen that the drift responses of uniform excitations provide a reliable estimate of the maximum response.

4.4. Deck Displacement

This part presents the relocation of the deck under-considered load cases and soil conditions. One of the most important elements of the long-span bridges that injured during past earthquakes is the deck. The failure patterns like beam failure or unseating from supports observed for failed bridges. Figure 15 illustrates the deck displacement in the transverse direction. The deck responses under non-uniform excitations are more than responses due to uniform excitations. The most unfavorable SVGMs component is the local site effects. Based on Figure 15 the maximum responses recorded under case 4 in which the soil condition changed from hard (abutments) to soft (middle columns). The effect of wave passage shows a rising trend. By getting far from the first simulation point the wave passage amplified the deck response. On the other side, the incoherence effect caused the deck response to be increased at the first and second simulation points. But by increasing

the distance from the first simulation point and scattering the traveling wave, the corresponding responses decreased. Comparing cases 4 and 5 confirmed that a strong incoherence parameter causes the deck responses to be reduced. Figure 16 (a), (b), (c), and (d), depict the total responses due to SVGMs and the contribution of pseudo-static components. From results, it is clear that pseudo-static responses cannot be ignored. Moreover, regarding Figure 16 (c) the soft soil beneath the foundations of the columns significantly increased the deck responses. The results of this part indicate that the bridge deck responses are sensitive to SVGMs.

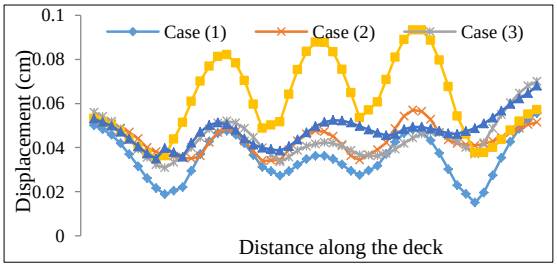

Fig. 15. Deck Displacement under various load and soil conditions.

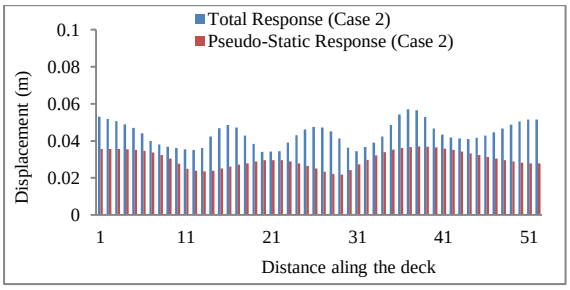

(a)

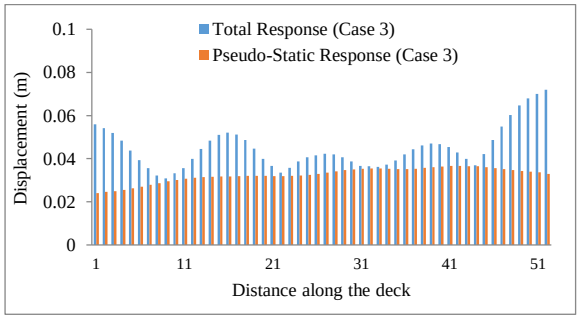

(b)

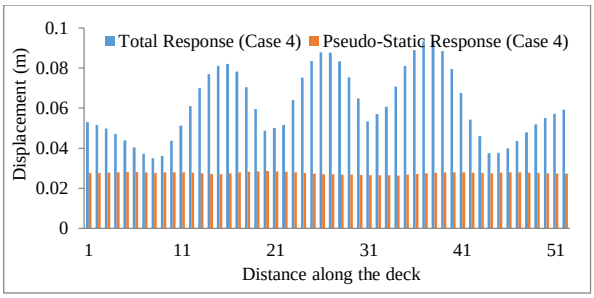

(c)

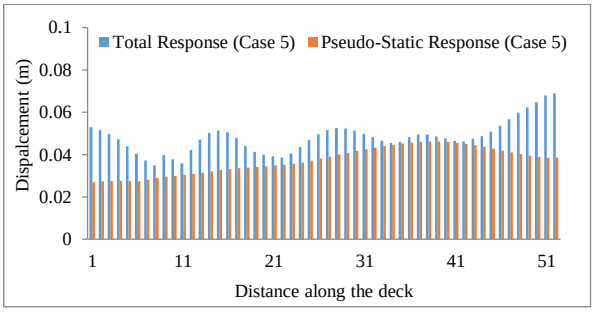

(d)

Fig. 16. Deck Displacement and relative pseudo-static contribution under various load and soil conditions.

4.5. Soil-Structure Interactions Effects

From previous studies, it is found that a soil-structure interaction (SSI) induces rotational foundations motions. For structures constructed on rigid foundations, the rotation of the mat can increase or decrease the dynamic response of the superstructure [42]. So, a simple model of springs, masses, and dashpots that illustrated in Figure 17, is utilized to explore the effect of SSI on the dynamic response of the bridge. Shear wave velocity considered based on Table 5 and the density of the soil assumed to be $\rho = 1800\ {}^{N}/_{m^3}$. Table 10 represents all parameters used to simulate the soil-structure interaction [43].

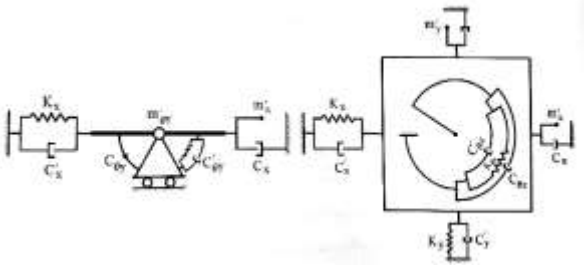

Fig. 17. Springs, masses and dashpots layout.

Figure 18; illustrates the deck displacement considering soil-structure interactions under different load and soil cases. Comparing with Figure 15, it is obvious that the responses due to uniform excitations remarkably increased. Except for the middle span, for the other parts of the deck, the maximum response occurred under uniform excitation. Among assumed load and soil scenarios, the results of case 4 are close to the results from uniform excitations with considering SSI. Figures 19 (a to d) represent the total and corresponding pseudo-static response of the deck to the assumed load and soil scenarios. Regarding the results obtained from the analysis without SSI effects, it is clear that soil structure interactions did not amplify the pseudo-static responses and the dynamic response significantly increased. Also, based on the results of the soil-structure interactions, it is clear that the responses increased.

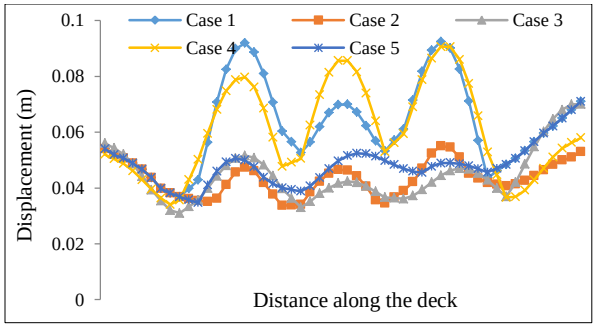

Fig. 18. Deck Displacement under various load and soil conditions considering SSI.

Table 10. Geometry and wave velocity of the cone model and coefficients of spring-dashpot-mass model [51].

Motion	Horizontal	Vertical	Rocking	Torsional
Equivalent radius r_0	$\sqrt{\frac{A_0}{\pi}}$	$\sqrt{\frac{A_0}{\pi}}$	$\sqrt[4]{\frac{4I_0}{\pi}}$	$\sqrt[4]{\frac{2I_0}{\pi}}$
Aspect ratio $\frac{z_0}{r_0}$	$\frac{\pi}{8}(2-\vartheta)$	$\frac{\pi}{4}(1-\vartheta)\left(\frac{c}{c_s}\right)^2$	$\frac{9\pi}{32}(1-\vartheta)\left(\frac{c}{c_s}\right)^2$	$\frac{9\pi}{32}$
Poisson's ratio υ	All ϑ	$\leq \frac{1}{3}$ $\frac{1}{3} < \vartheta < \frac{1}{2}$	$\leq \frac{1}{3}$ $\frac{1}{3} < \vartheta \leq \frac{1}{2}$	All ϑ
Wave velocity c	c_s	c_p 2	c_p $2c_s$	c_s
Trapped mass ΔM ΔM_θ	0	0 $2.4\left(\vartheta-\frac{1}{3}\right)\rho\, A_0\, r_0$	0 $1.2\left(\vartheta-\frac{1}{3}\right)\rho\, I_0\, r_0$	0
Discrete element model	$K=\rho\, c^2\, A_0/z_0$ $C=\rho\, c\, A_0$		$K_\theta=3\rho c^2\, I_0/z_0$ $C_\theta=\rho c I_0$ $M_\theta=\rho I_0 z_0$	

In which; $A_0$is foundation area, I_0 moment of inertia, Poisson's ratio ϑ, mass density ρ, shear-wave velocity, c_s, dilatational-wave velocity, c_p.

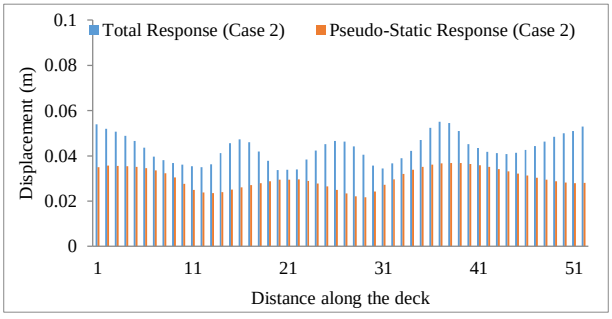

(a)

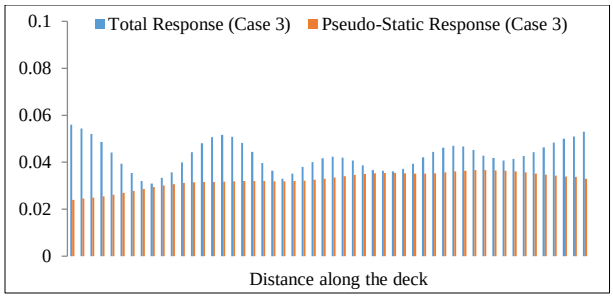

(b)

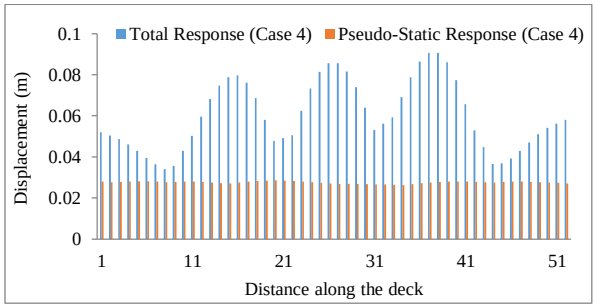

(c)

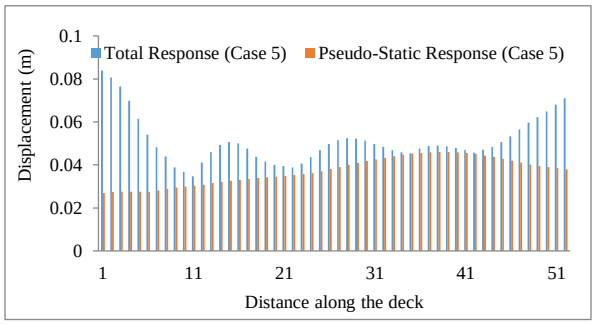

(d)

Fig. 19. Deck displacement and relative pseudo-static contribution under various load and soil conditions considering SSI.

5. Conclusions

In this study, a multiple support time history analysis of a reinforced concrete bridge was performed. A simulation technique to generate correlated arrays was explained and twenty series of correlated ground motions were simulated. From results, it is obvious that for long-span structures, the effect of SVGM must be included, and ignoring it may lead to a non-conservative design. The bridge was modeled by OpenSEES and excited under uniform and non-uniform load cases and soil conditions. The results of this study show that the response of long-span structures to SVGM can be more than the same results from uniform excitations. However, for short-span structures the responses reduce under SVGM excitations. Based on the results of this study;

1. Comparing results from cases 2 and 3 it can be concluded that for short distances, the most important SVGMs component is the incoherence parameter. Especially for short-bridges that situated on canyons the results of non-uniform excitations may be bigger than from uniform excitations.

2. The wave passage effect is more obvious in long-span structures with weak incoherency. Also, based on the results from cases 4 and 5, by decreasing the shear wave velocity (changing soil properties from hard to soft) the responses increase.

3. Non-uniform soil conditions (a combination of hard and soft soils for different supports) may make a destructive scenario for long-span structures such as river bridges.

4. From the results, the base shear response is not sensitive to SVGMs, and in all cases; the base shears response due to uniform excitations was more than results obtained from non-uniform excitations.

5. Based on the results, the axial forces of the columns affected by SVGM. It seems that the same response for cable-stayed or suspension bridges (cables elements) be more important. So, ignoring the SVGMs in designing of such elements is not safe.

6. The drift ratio of the columns under uniform and non-uniform excitations almost showed the same results and in some cases,

the results of uniform excitations were more than the same result from non-uniform. Also, from Figures 14, it is visible that the drift ratio on stiff soil is more than the same result on soft soil. So, it seems that for rigid systems (non-ductile) the response increases under non-uniform excitations.

7. The deck response is very sensitive to SVGM. In such a way that, for non-uniform soil conditions the responses of the deck significantly increased.

8. Regarding the outcomes, the most important SVGM component is local site effects. Non-uniform soil conditions and especially soft soil deposits strongly amplify the responses.

9. The results of the current study indicate that the Pseudo-Static components were induced some responses and confirmed that the effects of SVGM cannot be neglected.

10. Soil-structure interactions (foundation rotation) strongly amplified the dynamic responses and the results of the uniform excitations considering SSI effects and non-uniform excitations considering non-uniform soil conditions were very close. It is indicating that a combination of SVGM and SSI makes a very destructive scenario.

11. Overall, contrary to incoherency and wave-passage, that made moderate effects under non-uniform excitations, the site conditions generate a very noticeable effect on enhancing the structural response.

REFERENCES

[1] Leger, P., Ide, I. M. & Paultre, P. (1990). "Multiple-support seismic analysis of large structures", Computers & Structures, Vol. 36, No. 6, pp. 1153-1158. 10.1016/0045-7949(90)90224-P

[2] Nicholas J. Burdette, Amr S. Elnashai, F.ASCE, Allesio Lupi & Anastasios G. Sextos. (2008). "Effect of Asynchronous Earthquake Motion on Complex Bridges. I: Methodology and Input Motion. Journal of Bridge Engineering", 13-2. 10.1061/(ASCE)1084-0702(2008)13:2(158)

[3] Saxena V., Deodatis G. & Shinozuka M. (2000). "Effect of spatial variation of earthquake ground motion on the nonlinear dynamic response of highway bridges. Proc of 12th World Conf on Earthquake Engineering", Auckland, New Zealand.

[4] Vanmarcke EH, & Fenton GA. (1991). "Conditioned simulation of local fields of earthquake ground motion. Structural Safety", 10:247–264. 10.1016/0167-4730(91)90018-5

[5] Kameda. H, & Morikawa H.(1992). "An interpolating stochastic process for simulation of conditional random fields", Probabilistic Engineering Mechanics; 7:243–254. 10.1016/0266-8920(92)90028-G

[6] Liao S & Zerva A. (2006). "Physically compliant, conditionally simulated spatially variable seismic ground motions for performance-based design", Earthquake Engineering and Structural Dynamics; 35:891–919. 10.1002/eqe.562

[7] Konakli K. (2011). "Stochastic Dynamic Analysis of Bridges Subjected to Spatially Varying Ground Motions", A dissertation submitted in partial satisfaction of the requirements for the degree of Doctor of Philosophy, University of California, Berkeley.

[8] Morris NF. (1974). "Dynamic analysis of cable-stiffened structures", Journal of Structural Engineering Division ASCE. 100:971-81. https://cedb.asce.org/CEDBsearch/record.jsp?dockey=0022072

[9] Harichandran RS & WangW. (1990). "Response of one- and two- span beams to spatially varying seismic excitation", Earthquake Engineering and Structural Dynamics. 19: 2, 173-187. 10.1002/eqe.4290190203

[10] Falamarz-Sheikhabadi M.R. & Zerva A. (2016). "Effect of numerical soil-foundation-structure modeling on the seismic response of a tall bridge pier via pushover analysis", Soil Dynamics and Earthquake Engineering. 90:52–73. 10.1016/j.soildyn.2016.08.020.

[11] Apaydin NM., Bas S. & Harmandar E. (2016). "Response of the Fatih Sultan Mehmet Suspension Bridge under spatially varying multi-point earthquake excitations", Soil Dynamics and Earthquake Engineering. 84:44-54. 10.1016/j.soildyn.2016.01.018

[12] Adanur S., Altunisik AC., Soyluk K. & Bayraktar A. (2016). "Multiplesupport seismic response of Bosporus Suspension Bridge for various random vibration method", Case Studies in Structural Engineering. 5:54-67. 10.1016/j.csse.2016.04.001

dockey=0005745

[13] Falamarz-Sheikhabadi M.R. & Zerva A. (2017). "Analytical Seismic Assessment of a Tall Long-Span Curved Reinforced-Concrete Bridge. Part I: Numerical Modelling and Input Excitation", Journal of Earthquake Engineering, 21:1305–1334. 10.1080/13632469.2016.1211565.

[14] Falamarz-Sheikhabadi M.R. & Zerva A. (2018). "Two uncertainties in simulating spatially varying seismic ground motions: incoherency coefficient and apparent propagation velocity", Bull Earthquake Eng. 16:4427–4441. 10.1007/s10518-018-0385-x.

[15] Savvas P. Papadopoulos and Anastasios G. Sextos. "Anti-symmetric mode excitation and seismic response of base-isolated bridges under asynchronous input motion" Soil Dynamics and Earthquake Engineering 113 (2018) 148–161. 10.1016/j.soildyn.2018.06.004.

[16] Jian Zhong, Jong-Su Jeon and Wei-Xin Ren. (2018) "Risk assessment for a long-span cable-stayed bridge subjected to multiple support excitations. Engineering Structures. 176: 220–230. 10.1016/j.engstruct.2018.08.107

[17] Lufeng Zhao, Hong Hao, Kaiming Bi and Xiaozhen Li. (2018), "Numerical Study of the Seismic Responses of Precast Segmental Column Bridge under Spatially Varying Ground Motions" J. Bridge Eng. 23(12): 04018096. 10.1061/%28ASCE%29BE.1943-5592.0001319.

[18] Bas S., Apaydin N.M., Harmadar E. and Catbas N., (2018), "Multi-point earthquake response of the Bosphorus Bridge to site-specific ground motions", Steel and Composite Structures V. 26, N. 2, pages 197-211. 10.12989/scs.2018.26.2.197.

[19] Jeon J., Shafieezadeh A. and DesRoches R. (2018), "Component fragility assessment of a long, curved multi-frame bridge: Uniform excitation versus spatially correlated ground motions" Structural Engineering and Mechanics, V. 65, N. 5, 2018, pages 633-644. 10.12989/sem.2018.65.5.633.

[20] Yurdakul M. and Ates S. (2018) "Stochastic responses of isolated bridge with triple concave friction pendulum bearing under spatially varying ground motion", Structural Engineering and Mechanics. V. 65, N. 6, pages 771-784. 10.12989/sem.2018.65.6.771.

[21] Tonyali Z., Ates S. and Adanur S. (2019) "Spatially variable effects on seismic response of the cable-stayed bridges considering local soil site conditions", Structural Engineering and Mechanics. V. 70, N. 2, pages 143-152. 10.12989/sem.2019.70.2.143.

[22] Shiravand M.R. and P. Parvanehro. (2019), "Spatial variation of seismic ground motion effects on nonlinear responses of cable stayed bridges considering different soil types", Soil Dynamics and Earthquake Engineering. 119: 104–117. 10.1016/j.soildyn.2019.01.002.

[23] Payganeh.M.B. and Mortezaei. A. (2020). "Seismic damage assessment of RC buildings subjected to the rotational ground motions records considering soil-structure interaction", Journal of Rehabilitation in Civil Engineering. 8-2, 62-80. 10.22075/jrce.2019.17206.1319

[24] Konakli K. and Der Kiureghian A. (2012). "Simulation of spatially varying ground motions including incoherence, wave-passage and differential site-response effects", Earthquake Engineering and Structural Dynamics. 41-3. 495-513. 10.1002/eqe.1141.

[25] Anderson TW. (1971). "The Statistical Analysis of Time Series". John Wiley & Sons, Inc. New York. 10.1002/9781118186428

[26] Zerva A & Harada T. (1994). "A site-specific model for the spatial incoherence of the seismic ground motions". Proceedings of the 5th National Conference on Earthquake Engineering, Chicago, Illinois.

[27] Chatfield C. (2004). "The Analysis of Time Series: An Introduction". CRC Press LLC: Boca Raton, Florida.

[28] Abrahamson NA., Schneider JF., & Stepp JC. (1991). "Empirical spatial coherency functions for applications to soil-structure interaction analyses", Earthquake Spectra. 7, 1–27. 10.1193/1.1585610

[29] Harichandran RS & Vanmarcke EH. (1986). "Stochastic variation of earthquake ground motion in space and time", Journal of Engineering Mechanics. Div. 112,154–174. 10.1061/(ASCE)0733-9399(1986)112:2(154)

[30] Zerva A. & Zervas V. (2002). "Spatial variation of seismic ground motions: An overview", Application Mechanic, vol 55, no 3.

[31] Novak M. & Hindy A. (1979). "Seismic response of buried pipelines". 3rd Canadian Conf on Earthquake Engineering, Montreal Canada.

[32] Der Kiureghian A. & Neuenhofer A. (1992). "Response spectrum method for multiple support seismic excitation", Earthquake Eng.Struct. Dyn. 21, 713–740. 10.1002/eqe.4290210805

[33] Luco JE. & Wong HL. (1986). "Response of a rigid foundation to a spatially random ground motion". Earthquake Engineering and Structural Dynamics; 14:891–908. 10.1002/eqe.4290140606

[34] Ketchum M., Chang V. & Shantz T. (2004). "Influence of design ground motion level on highway bridge costs". 04:6D01. Pacific Earthquake Engineering Research Center, Berkeley, CA, USA.

[35] McKenna F. & Fenves GL. (2000). "An object-oriented software design for parallel structural analysis". In: Proceedings of the advanced technology in structural engineering. Structures Congress 2000, ASCE,Washington,DC.

[36] Taucer F., Spacone E. & Filippou FC. (1991). "A fiber beam–column element for seismic response analysis of reinforced concrete structures". Earthquake Engineering Research Center, College of Engineering, University of California, Berkeley.

[37] Tondini N. & Stojadinovic B. (2012). "Probabilistic seismic demand model for curved reinforced concrete bridges". Bull Earthquake Eng. 10: 1455-1479. 10.1007/s10518-012-9362-y

[38] Amjadian M. & Agrawal A. K. (2017). "Dynamic characteristics of horizontally curved bridges". Journal of Vibration and Control. 1–19. 10.1177/1077546317726637

[39] Zhang J. & Makris N. (2002a). "Kinematic response functions and dynamic stiffness of bridge embankments". Earthq Eng Struct Dyn, 31:1933–1966. 10.1002/eqe.196

[40] Zhang J., Makris N. & Delis E. (2004). "Structural characterization of modern highway overcrossings-a case study". J. Struct Eng ASCE. 130(6):846–860. 10.1061/(ASCE)0733-9445(2004)130:6(846)

[41] Anestis S. V. & Damodaran N. (1975). "Seismic Interaction of Structures on Hysteretic Foundations". Journal of the Structural Division. 101, 1, 109-129. https://cedb.asce.org/CEDBsearch/record.jsp?

[42] Toki K. & Yanabu K. (1988). "Detection of apparent wave velocity in near surface ground with irregular profile by an array observation". Proceeding of 9th world conf on earthquake engineering, Tokyo.

[43] Wolf John P. (1997). "Spring-Dashpot-Mass Models For Foundation Vibrations". Earthquake Engineering and Structural Dynamics, 26, 931-949. 10.1002/(SICI)1096-9845(199709)26:9<931::AID-EQE686>3.0.CO;2-M